International Journal of Engineering Research & Technology (IJERT)
ISSN: 2278-0181
Vol. 9 Issue 02, February-2020

Spectroscopic and Computational Analysis of 4-Methoxythioanisole

Akhil.R.Krishnan,
Department of Physics,
Malabar Christian College,
Calicut, Kerala, 673001

H.Saleem,
Department of Physics,
Annamalai University,
Annamalai Nagar, 608 002

K. Jayakumar, D.Nandhini, S.Subashchandrabose
Centre for research & Development,
PRIST Deemed University,
Vallam, Thanjavur, 613403

ABSTRACT:- In this work a joint experimental and theoretical study on 4-Methoxythioanisole (4-MTA) is reported. Detailed analysis of the FT-Raman, FT-IR and NMR spectra of 4-MTA has been performed. In parallel, quantum chemical calculations based on DFT (B3LYP) methods were used to determine the geometrical, energetic and vibrational characteristics of the molecule and complete assignments were performed on basis of the analysis of the potential energy distribution (PED) of the normal modes. The theoretical spectra were refined using scaled quantum mechanics force field (SQM-FF) method as well as the uniform scaling approach. NBO analysis was applied to understand the intramolecular hyperconjugative interactions between bonding and anti bonding orbital. The Mulliken population analysis on atomic as well as on the NBO charges, and the HOMO–LUMO energy are calculated, besides the molecular electrostatic potential (MEP), thermodynamic properties are also reported.

1. INTRODUCTION

In the past anisole has been investigated as a key molecule for the description of a number of molecular properties due to the possibility of torsion of the methoxy group with respect to the aromatic ring. Anisole was taken as the parent molecule for reference in a systematic study on disubstituted aromatic molecules [1, 2] and more recently it has been considered as a model system for the study of intermolecular interactions due to the presence of the polar methoxy group. This group is able to form hydrogen bonded networks, due to the non-bonding electron density at the oxygen atom, but only as a proton acceptor. There is the possibility of obtaining detailed information from these complexes about both intermolecular interaction and the dynamics of chemical reactions [3]. Anisole, anisic acid and their derivatives are widely used in chemical reaction as intermediates to obtain target materials such as dyes, pharmaceuticals, perfumes, photo initiators and agrochemicals. Spectroscopic investigation of anisole [4, 5] and its derivatives has received considerable attention as the former is a representative model compound for a number of chemically and biologically interesting systems.

Many attempts have been made to study the various types of spectra arising from anisole and its substituents. Calculation of the structures, stabilities and vibrational spectra of arsenates, thioarsenites and thioarsenates in aqueous solution was performed by Tossell et al., [6]. Mariko et al., [7] studied the molecular structure of jet-cooled thioanisole by laser-induced fluorescence spectroscopy and *ab initio* calculations. Vibrational analysis and theoretical calculations of p-methylanisole in the first electronically excited S_1 and ionic ground D_o states were carried out by Jianou et al., [8]. Krishnakumar et al., [9] reported the scaled quantum chemical studies of the structure and vibrational spectra of 2-(methylthio) benzimidazole

The rotational isomerism of anisole and thioanisole was investigated by Mario et al., [10] on the basis of computational methods within the framework of the Moller-Plesset and density functional theory. Venkatram et al., [11] studied the transferable valence forcefields for substituted benzenes and vibrational analysis of substituted anisole was carried out by Lakshmaiah et al., [12]. A Raman spectroscopic study of the low-frequency vibrations in anisole-d5 and anisole-d8 is conducted by Tylli et al., [13].

The literature survey reveals that thioanisole and its derivatives have attracted many researchers. In this work we report the FT-IR, FT-Raman and NMR spectral analysis of 4-MTA utilizing DFT (B3LYP). Vibrational spectral analysis has been done using B3LYP with several basis sets. The bands assignment is based on PED. The minimum energy conformational analysis was carried out with the help of potential energy surface scan. The redistribution of electron density (ED) in various bonding and antibonding orbitals and E2 energies has been calculated by natural bond orbital (NBO) analysis using the DFT method to give clear evidence of stabilization originating from the hyper conjugation of various intra-molecular interactions. HOMO and LUMO analysis has been used to elucidate information regarding charge transfer within the molecule. Furthermore, the electric dipole moment μ_{tot}, isotropic polarizability α_{tot}, finite hyperpolarizability β_{tot}, and also the molecular electrostatic potential (MEP) for the title molecule are also evaluated from the computational process.

(This work is licensed under a Creative Commons Attribution 4.0 International License.)

International Journal of Engineering Research & Technology (IJERT)
ISSN: 2278-0181
Vol. 9 Issue 02, February-2020

2. EXPERIMENTAL DETAILS

The compound 4-MTA in the liquid form was purchased from Sigma-Aldrich Chemical Company (USA) with a stated purity greater than 98% and was used as such without further purification. The FT-Raman spectrum of 4-MTA was recorded using the 1064 nm line of a Nd:YAG laser as excitation wavelength in the region 10-3500 cm^{-1} on a Bruker model RFS 100/S spectrophotometer. The FT-IR spectrum of this compound was recorded in the region 400-4000 cm^{-1} on an IFS 66V spectrophotometer using NaCl Cell and standard Ge as detector. The spectra were recorded at room temperature, with a scanning speed of 10 cm^{-1} per minute and at the spectral resolution of 2.0 cm^{-1}. The theoretically predicted scaled IR and Raman spectra at B3LYP/6-311/6-311++G(d,p) level of calculations along with experimental FT-IR and FT-Raman spectra are shown in Figs.1 and 2. NMR spectra were also measured in DMSO at ambient temperature on a Varian Mercury-VxBB 300 spectrometer (299.95 MHz for ^{1}H and 75.43 MHz for ^{13}C). The FT-IR and FT-Raman spectral measurements were carried out at Sree Chitra Tirunal Institute for Medical Sciences and Technology, Thiruvananthapuram, Kerala and NMR is taken from RSIC, IIT, Chennai.

3. COMPUTATIONAL DETAILS

For meeting the requirements of both accuracy and computing economy, theoretical methods and basis sets should be considered. DFT has proved to be extremely useful in treating electronic structure of molecules. The density functional three parameter hybrid model (DFT/B3LYP) at several basis set levels was adopted to calculate the properties of the studied molecule. All the calculations were performed using the Gaussian 03W and Gaussian 09 RevA.02 program packages [14] with the default convergence criteria without any symmetry constraints [15].

The energetically minimal geometry was taken from the PES scan computations - described below - and the starting geometry has been further optimized at the each level of theory. Vibrational analysis confirmed that all the structures studied in this work were true minima on PES, since no imaginary frequencies were observed.

3.1. Potential Energy Scan

When neglecting the methyl groups, due to their very low energy barrier for reorientation which is normally present even in the solid state, the conformational problem of 4-MTA may be strictly related only to the orientation of the substituents. The two dimensional relaxed potential energy surface scan, using internal redundant coordinates (through the Opt=ModRedundant option), has been performed for the angles C12-S11-C1-C6 and C5-C4-O16-C17 at the B3LYP/6-31G(d) level of theory, using Gaussian 09. The initial geometry was symmetrized, assuming the ideal symmetry of the phenyl ring, and the relaxed scan was performed at every 30.0° in the range of 0.0-360.0° for each angle. The resulting grid including 169 points is plotted in Fig.3. The energy values for each point were recounted into kJ/mol with respect to the lowest energy grid point.

The PES scan clearly reveals that the only stable conformation corresponds to the sharp, iso-energetic minima. The minima define the orientation of CH_3-S-Ph and CH_3-O-Ph groups to be, respectively, almost ideally perpendicular and parallel with respect to the phenyl ring plane. The four minima correspond to the stable conformers which are however energetically degenerated and equivalent by the local symmetry. As a result, the corresponding spectra are undistinguishable. The energy barriers for the rotation over –S-Ph- and –O-Ph- bonds may be estimated by B3LYP/6-31G(d) as ~3.2 and 14.4 kJ/mol, respectively. Such a low energy barrier for the rotation about the C-S bond may suggest that the deformation of this molecular part may be easily expected in the solid state, especially taking into account the occurence of π-π stacking interactions. Since, there is no hydrogen bonding expected in the studied system, which is rather mainly driven by London forces, we can compare this energy barrier, with a kT value at standard conditions, which may be estimated as 2.48 kJ/mol. Although the applied theory level is not of the highest quality, and the approximation is straightforward, it suggests that the reorientation disorder of this molecular fragment may be present at room temperature. The results might suggest that such disorder plays a crucial role in the crystal melting which occurs just below the room temperature (22-23 ºC). In comparison, it is much lower than 4-MTA, which melts c.a. 56-60 ºC. This difference is also shown by the computed energy barrier for the rotation about the C-O bond, which is also much higher.

3.2. Vibrational analysis

B3LYP at several- double and triple-ζ basis set levels has been applied to study the theoretical vibrational spectrum of 4-MTA. A detailed description of vibrational modes can be given by means of normal coordinate analysis (NCA). NCA analysis based on the SQM-ff method was performed using MOLVIB program ver. 7 [16, 17] written by T. Sundius, delivering the potential energy distribution contributions of each normal mode, their corrected frequencies and the recomputed infrared and Raman intensities after scaling of the force field. For this purpose, the full set of 68 standard internal valence coordinates (containing 14 redundancies) has been defined as given in Table.1. From these, a non-redundant set of local internal coordinates was constructed (Table.2) much like the 'natural internal coordinates' recommended by Fogarasi and Pulay [18, 19, 20] The theoretically calculated DFT force fields were transformed to this latter set of vibrational coordinates and used in all subsequent calculations.

The SQM calculations were performed based on the Pulay's method, according to which the internal force constants f_{ij} are transformed according to geometric mean scaling:

$$f_{ij}^{'} = \sqrt{S_i S_j}\, f_{ij} \qquad (1)$$

(This work is licensed under a Creative Commons Attribution 4.0 International License.)

International Journal of Engineering Research & Technology (IJERT)
ISSN: 2278-0181
Vol. 9 Issue 02, February-2020

Where S_i denotes a scaling constant. In the application of the method the non-diagonal terms in the potential energy depend nonlinearly on the scale factors. The MOLVIB SCALE=1 option has been chosen, what means that the factor $\sqrt{S_i S_j}$ that occurs in front of the non-diagonal force constant is fixed during the iteration.

The SQM adjusted Raman activities (A_i) were then transformed into the Raman intensities (I_i), using the relationship derived from the theory of Raman scattering [21].

$$I_i = \frac{f(\nu_0 - \nu_i)^4 A_i}{\nu_i \left[1 - \exp\left(\frac{-hc\nu_i}{kT}\right)\right]} \quad \textbf{(2)}$$

Where ν_0 is the exciting wavenumber (in cm^{-1}), ν_i the SQM corrected frequency of the i^{th} normal mode; h,c and k are the fundamental constants; and T is the temperature (298 K), f is a suitably chosen common scaling factor for all the peak intensities.

The SQM-ff vibrational analysis with B3LYP was performed at the following basis set levels: 6-31G(d), 6-31+G(d), 6-311+G(d,p) and 6-311++G(d,p). The applied sets of transferable scale factors were taken from the literature without further refinement, except of 6-311++G(d,p). V. Krishnakumar refined the classic Pulay-Rauhut 6-31G(d) scale factors [22] which were also applied here, for the for the triple-ζ quality force fields, and has shown the very good agreement for the calculations with an analogous compound [23] R. Korlacki has also proofed that the scale factors refined for B3LYP/6-31+G(d) work extremely well for very large, liquid crystalline polyatomic thiobenzoates [24] In the case of 6-311++G(d,p) basis set, the quoted Pulay-Rauhut 6-31G(d) scale factors were refined with respect to the assigned experimental bands. Since, the experimental spectra are not very rich in bands, most of the similar coordinates were grouped together and finally seven scale factors were chosen for refinement. The error of one scale factor connected with some of the torsions was rather high, so the torsional coordinates were further combined and finally, the total number of scale factors was reduced to six. In the case of 6-311+G(d,p) and 6-311++G(d,p) the uniform scaling factor of 0.9679, which was suggested for the computations at the quoted levels, has also been applied for comparison [25] The PED was calculated for the scaled force field obtained with B3LYP/6-311++G(d,p) theory level and the experimental results were interpreted on the basis of these results. All the computed wavenumbers were collected together and presented in Table.S1 along with calculated root mean square deviation values (RMSD), PED contributions for each normal mode, and the band assignment.

3.3. Hyperpolarizability calculations

The first hyperpolarizabilities (β, α_0 and Δα) of 4-MTA were calculated at the B3LYP/6-31G(d,p) level, based on the finite-field approach. In the presence of an applied electric field, the energy of a system is a function of the electric field. First hyperpolarizability is a third rank tensor that can be described by a 3x3x3 matrix. The 27 components of the 3D matrix can be reduced to 10 components due to Kleinman symmetry [26]. It can be given in the lower tetrahedral format. It is obvious that the lower part of the 3x3x3 matrixes is a tetrahedral. The components of β are defined as the coefficients in the Taylor series expansion of the energy in the external electric field. When the external electric field is weak and homogeneous, this expansion becomes:

$$E = E^0 - \mu_\alpha F_\alpha - 1/2\alpha_{\alpha\beta}F_\alpha F_\beta - 1/6\beta_{\alpha\beta\gamma}F_\alpha F_\beta F_\gamma + \ldots \quad (3)$$

Where E^0 is the energy of the unperturbed molecules, F_α is the field at the origin, and $\mu_\alpha, \alpha_{\alpha\beta}, \beta_{\alpha\beta\gamma}$ are the components of the dipole moment, polarizability and the first hyperpolarizabilities, respectively. The total static dipole moment μ, the mean polarizability α_0, the anisotropy of polarizability $\Delta\alpha$ and the mean first hyperpolarizability β_0, using the *x, y, z* components are defined as

$$\mu = \left(\mu_x^2 + \mu_y^2 + \mu_z^2\right)^{1/2} \quad (4)$$

$$\alpha_0 = \frac{\alpha_{xx} + \alpha_{yy} + \alpha_{zz}}{3} \quad (5)$$

$$\Delta\alpha = 2^{-1/2}\left[\left(\alpha_{xx} - \alpha_{yy}\right)^2 + \left(\alpha_{yy} - \alpha_{zz}\right)^2 + \left(\alpha_{zz} - \alpha_{xx}\right)^2 + 6\left(\alpha_{xy}^2 + \alpha_{yz}^2 + \alpha_{xz}^2\right)\right]^{1/2} \quad (6)$$

$$\beta_0 = \left(\beta_x^2 + \beta_y^2 + \beta_z^2\right)^{1/2} \quad (7)$$

The total molecular dipole moment (μ) and mean first hyperpolarizability (β) are given in Table.3 and equal 1.0402 Debye and 3.1300 x 10^{-30} esu, respectively. The total dipole moment is approximately equal and the first hyperpolarizability of the title molecule is eight times greater than that of urea (μ and β of urea are 1.3732 Debye and 0.3728 x 10^{-30}).

(This work is licensed under a Creative Commons Attribution 4.0 International License.)

International Journal of Engineering Research & Technology (IJERT)
ISSN: 2278-0181
Vol. 9 Issue 02, February-2020

4. RESULTS AND DISCUSSION

4.1. Molecular Geometry

The optimized geometrical parameters of the title molecule are given in the Table.S2 using B3LYP/6-311G(d,p)/6-311++G(d,p) methods. The optimized molecular structure of 4-MTA is shown in Fig.4 with the atom numbering adopted in this work. Since the exact molecular structure of the compound is not available, the calculated geometry of 4-MTA is compared with available gas electron diffraction data of thioanisole [27]. From the Table.S1 it is evident that the electron donating tendency of sulphur influences the bond length as well as the bond angle values. The optimized bond length of C_1-S_{11} in 4-MTA is 1.795 and 1.785 Å by B3LYP 6-311/6-311++G(d,p) and HF (6-311++G(d,p)) respectively. On the other hand from gas electron diffraction data of thioanisole the C_1-S_{11} bond length is predicted as 1.813 Å, which deviates by ~ 0.028Å from the theoretical value. The bond angles of the six membered carbon ring are usually less than or equal to 120°. In the present investigation, the optimized bond angle of 4-MTA is obtained at 120.7° for C1-C2-C3 and C1-C6-C5, while the C2-C1-S11 bond angle is obtained as 120.5°. The bond parameters calculated by the theoretical methods are more or less equal to the available experimental data.

4.2. Vibrational assignment

The total number of atoms in this molecule is 20 which give 54 (3N-6) normal modes. The molecule belongs to the C_1 point group, thus all the 54 fundamental vibrations, are by definition both IR and Raman active. The vibrational spectral analysis has been carried out on basis of the FT-IR, FT-Raman measurements in combination with the computed vibrational frequencies**.** Vibrational mode assignments have been made on the basis of the relative intensities, the wavenumbers and PED contributions. A good correlation was found between the computed and the experimental spectra, which confirms that no significant specific interactions may be found in the studied system. The calculated vibrational wavenumbers, measured FT-IR and FT-Raman band positions and the calculated PED's for each normal mode are presented in Table.S1. Experimental frequencies are compared with all the theoretical wavenumbers delivered by previously mentioned procedure. The presented PED's obtained for the SQM scaled force fields were derived from B3LYP/6-311++G(d,p) computations, where the scale factors were refined with respect to the present experiment. As may be seen in the table, the application of SQM gives certainly better results than the simple uniform frequency scaling. However, the S-C stretching frequency has been predicted poorly by the quoted level what increases the estimated RMSD. Moreover, the further refinement might bring even better improvement, but since the recorded data are not rich in bands and the Raman spectrum is quite noisy, it would not be possible to construct a more complex set of scale factors. The experimental spectra are plotted versus the quoted theory level in Figs.1. and 2**.** All the computations delivered very similar intensity relations. Application of SQM had also negligible influence on the calculated PED's, which were derived from the B3LYP/6-311++G(d,p) results. The whole discussion presented below is based on the quoted SQM theory level.

For the better understanding, vibrational modes have been discussed under separate headings viz. C-H vibrations, ring vibrations, CH_3 vibrations, C-O vibrations and C-S vibrations.

4.2.1. C-H vibrations

Aromatic compounds commonly exhibit multiple weak bands in the region 3100-3000 cm^{-1} due to aromatic C-H stretching vibrations [28]. Our title compound 4-MTA has one aromatic ring as shown in Fig.4. The scaled vibrations, [modes: 54-52] which are assigned to aromatic C-H stretching, and computed in the range 3050-3077 cm^{-1} show good agreement with the recorded very weak FT-IR line at 3080 cm^{-1} and strong FT-Raman line at 3081 cm^{-1}. As expected these four modes are pure stretching modes as it is evident from the PED column. Their contribution from C-H stretch is close to 100%. Although the computations were performed in harmonic approximation, the application of SQM delivered a partial compensation of the errors given by simplified vibrational approach.

In the benzene ring, the C-H in-plane bending vibrations most often lay in the region 1230-970 cm^{-1} [28]. In 4-MTA the band of medium strong intensity, observed in the FT-IR spectrum at 1290 cm^{-1}, as well as the weak one at 1106 cm^{-1} were assigned to the C-H in-plane bending vibrations, strongly mixed with the □CCar stretching modes. The former mode manifests also as a weak band in the Raman spectrum. The most intensive band in the FT-IR spectrum at 1504 cm^{-1} is also related to the in-plane bending vibration (48% in PED) significantly coupled with the ring stretching vibration (33% in PED).

The bands observed at 826 and 805 cm^{-1} in FT-IR are assigned to C-H out-of-plane bending vibrations. These assignments show good agreement with theoretically scaled harmonic wavenumber values at 829 and 803 cm^{-1}.

4.2.2. Ring vibrations

Several ring vibrations are affected by substitution to the aromatic ring of benzene. Benzene ring vibrations are found to make a major contribution in the IR and Raman spectra of the sample. Benzene ring stretching vibrations usually occur in the region 1580-1300 cm^{-1} [29, 30]. For aromatic six membered rings, eg. benzene and pyridines, there are two or three bands in this region due to skeletal vibrations, the strongest usually being at about 1500 cm^{-1}. In the case where the ring is conjugated, a further mode at 1580 cm^{-1} is also observed. For substituted benzene with identical atoms or groups on all para-pairs of ring carbon atoms, the vibrations giving rise to the band at 1625-1590 cm^{-1} are infrared inactive due to symmetry considerations, the compound having a centre of symmetry at the ring centre. If the groups in para positions of carbon atoms are different, then there is no centre of symmetry and the vibrations are infrared-active [31].

(This work is licensed under a Creative Commons Attribution 4.0 International License.)

International Journal of Engineering Research & Technology (IJERT)
ISSN: 2278-0181
Vol. 9 Issue 02, February-2020

The ring C-C stretching vibrations occur in the region 1650-1400 cm^{-1} [32]. In the present work, the bands at 1604, 1583, 1504, 1246 cm^{-1} in FT-IR and the strong band at 1598 cm^{-1}, along with the above mentioned weak band at 1292 cm^{-1} in FT-Raman are assigned to C-C stretching vibrations, staying in good agreement with the theoretically computed values at 1599, 1572, 1487, 1286, 1244 cm^{-1}.

The calculated ring symmetric and asymmetric deformations may be probed by Raman spectroscopy. According to the theory, the symmetric modes may be found at 801 and as a strongly mixed mode at 344 cm^{-1}, while the asymmetric ones may be found at 650 and 307 cm^{-1}. It is experimentally confirmed by the presence of the bands at 798 and 338; 633 and 309 cm^{-1} as well as with the literature values [33].

The torsional deformations contribute significantly to the vibrations observed below 800 cm^{-1}. These bands were observed via FT-RS spectroscopy at 551 and 208 cm^{-1}, however the related modes are strongly mixed mainly with the out-of-plane deformations of the substituents. The theoretically predicted band at 709 cm^{-1} corresponds to the Rtrig torsional deformation. However, this mode was not observed experimentally due to the high intensity of near laying C-S mode.

4.2.3. CH_3 vibrations

The title molecule possesses two CH_3 groups as shown in Fig.4. For the assignments of CH_3 group frequencies, basically nine fundamentals can be associated to each CH_3 group namely; the symmetrical stretching, asymmetrical stretching, the symmetrical, asymmetrical deformation modes, in-plane rocking, out-of-plane rocking and twisting modes. The C-H stretching modes in CH_3 occur at lower frequencies than those of aromatic ring. In theory, the asymmetric C-H stretching modes were found in the range 3009-2942 cm^{-1} [mode no's: 50-47] while the symmetric C-H stretching modes at 2917 and 2885 cm^{-1}. These wavenumbers are supported by the experimental bands found at 3016, 2934, 2853 cm^{-1} in FT-IR and 3013, 2936, 2856 cm^{-1} in FT-Raman spectra, respectively. These assignments are also supported by the literature [34] in addition with the PED analysis.

For methyl substituted benzene derivatives, the asymmetric and symmetric deformation vibration of the methyl group normally appear in the region 1465-1440 cm^{-1} and 1390-1370 cm^{-1} respectively [35, 36, 37].

The theoretically predicted frequency at 1325 cm^{-1} [mode no: 36] was assigned to symmetric deformation vibration of CH_3 group and are in good agreement with the above literature data. The in-plane bending vibrations of the CH_3 group have been identified theoretically at 1458 and 1447 cm^{-1}, staying in very good agreement with the experimental values found at 1445 cm^{-1} and 1449 cm^{-1} in the FT-IR and FT-RS spectra, respectively. The out of plane bending vibration manifest in the experimental infrared spectrum as a band of medium intensity at 1470 cm^{-1}, staying in the excellent agreement with the theoretically predicted value of 1469 cm^{-1}.

The rocking vibrations of CH3 mode usually appear in the region 1070-1010 cm^{-1} [38]. The theoretically computed frequencies are spread over the range 1175-948 cm^{-1}. The upper energy vibrations correspond to the rocking modes of the methoxy group. The strong bands recorded at 1183 (strong in FT-IR) and 1178 cm^{-1} (medium-strong in FT-RS) are linked to the out-of-plane methoxy rocking (53% in PED), while the in-plane rocking vibration is assigned to the weak band observed via FT-IR at 1121 cm^{-1}. The weak band found at 972 cm^{-1} in FT-IR has been assigned to S-CH3 rocking vibrations.

4.2.4. C-O and C-S vibrations

The characteristic alkoxy group vibrations are C-O stretching and C-O bending vibrations. They are expected in the region 1140-395 cm^{-1} and 1700-875 cm^{-1} depending on the presence of specific interactions, whether monomeric, dimeric or other hydrogen bonded species are present [38]. However, these bands overlap with other due to aromatic or aliphatic chain vibrations. Hence their undisputed assignment is often very difficult [38]. Here, it is clearly reflected in presented PED, where the vibrations involving alkoxy bridge reveal strongly coupled character. In our present investigation, the strong bands observed at 1246 (vs) and 1034 (s) cm^{-1} in FT-IR are assigned to C-O stretching, being well supported by the theoretical values of 1231 and 1023 cm^{-1} with the dominant contributions of CarO in PED equal 42 and 68%, respectively. The weak band observed at 1121 and 1183 cm^{-1} in FT-IR and the one at 1178 cm-1, corresponding to the latter in FT-Raman spectrum are assigned to OCH3 in- and out-of-plane bending and they are all well supported by the theoretical and literature values. Most of the C-S vibrations are manifested by the theory below 750 cm^{-1}. Being strongly mixed, the modes cannot be treated separately. However, the most characteristic band, related to the C-S stretching may be observed in Raman spectrum at 717 cm^{-1}. The band should be of weak intensity in infrared, however being of very strong intensity in Raman spectrum [39]. The corresponding theoretical value differs significantly, giving the wavenumber of 672 cm^{-1} with almost pure relation to the C-S stretching coordinate with the PED contribution of 91%. All the tested theory levels brought similar fail in the prediction of the quoted frequency, however applying the set of scale factors defined by Krishnakumar et. al leads to the closest value 694 cm^{-1}. It suggests that the fail may be due to a systematic error delivered by the selected level of theory

4.3. NMR Analysis

In proton NMR spectrum of the title compound, two signals at 2.41 and 3.72 ppm with each three protons integral are assigned to S-CH_3 and OCH_3 protons respectively. Likewise in aromatic region, oxygen adjacent two aryl protons are resonated as a singlet at 7.23 ppm with two protons integral and sulphur adjacent protons appeared as a singlet at 6.89 ppm with two protons integral. This deshielding and shielding of aryl protons are due to the electro negativity of oxygen and sulphur atoms respectively.

(This work is licensed under a Creative Commons Attribution 4.0 International License.)

International Journal of Engineering Research & Technology (IJERT)
ISSN: 2278-0181
Vol. 9 Issue 02, February-2020

In ^{13}C NMR spectrum, a less intense signal at 158.08 ppm is assigned to OCH_3 bearing ipso carbon whereas two signals at 129.62 and 115.14 ppm are due to the oxygen attached to two aryl carbons and sulphur attached two aryl carbons respectively. In the up field region, a signal at 55.54 ppm is assigned to OCH3 carbon and a signal at 17.13 ppm is attributed to SCH_3 carbon. The molecular structure of the MTA molecule was optimized. Then, gauge-including atomic orbital (GIAO) ^{13}C NMR and ^{1}H NMR chemical shifts calculations of the 4-MTA molecule were carried out by using B3LYP functional with 6-311++G(d,p) basis sets. The NMR spectra calculations were performed by using the Gaussian 09 [14] program package. The calculations reported were performed in DMSO solution using the IEF-PCM model, rather than in the gas phase, in agreement with experimental chemical shifts obtained in DMSO solution. The experimental and calculated values for ^{13}C and ^{1}H NMR are shown in Table.4. The observed ^{1}H and ^{13}C NMR spectra of 4-MTA is plotted in Fig.5.

4.4. NBO ANALYSIS

Natural bond orbital analysis gives the most accurate possible natural Lewis structure picture of ø because all orbitals are mathematically chosen to include the highest possible percentage of the ED. Interaction between both filled and virtual orbital spaces information is correctly explained by the NBO analysis and it could enhance the analysis of intra and inter-molecular interactions. The second order perturbation theory analysis of the Fock matrix was carried out to evaluate donor (i) – acceptor (j) i.e. donor level bonds to acceptor level bonds interaction in the NBO analysis [40]. The result of interaction is a loss of occupancy from the concentration of electron NBO of the idealized Lewis structure into an empty non-Lewis orbital. For each donor (i) and acceptor (j), the stabilization energy E (2) associated with the delocalization i → j is estimated as

$$E^{(2)} = \Delta E_{ij} = q_i \frac{F(i,j)^2}{\varepsilon_j - \varepsilon_i} \qquad (8)$$

Where q_i is the donor orbital occupancy, ε_j and ε_i are diagonal elements and F(i, j) is the off diagonal NBO Fock matrix element. Natural bond orbital analysis provides an efficient method for studying intra and inter-molecular bonding and interaction among bonds, and also provides a convenient basis for investigating charge transfer or conjugative interaction in molecular systems. Some electron donor orbital, acceptor orbital and the interacting stabilization energy resulting from the second-order micro-disturbance theory are reported [41, 42]. The larger E(2) value, the more intensive is the interaction between electron donors and acceptor, i.e. the more donation tendency from electron donors to electron acceptors and the greater the extent of conjugation of the whole system [43]. Delocalization of ED between occupied Lewis – type (bond or lone pair) NBO orbitals and formally unoccupied (anti bond or Rydberg) non Lewis NBO orbital correspond to a stabilizing donor-acceptor interaction.

The charge transfer during the inter-molecular interaction shows the delocalization of energy from one bond to another. The C_1-C_6 bond has σ* and π* type electrons and its densities are 1.9787 and 1.6750 respectively. The lower bond density shows more stabilization due to higher occupancies in acceptor bonds. It is evident that the transfers from C_1-C_6, C_2-C_3 and C_4-C_5 to its antibonding orbitals of C_1-C_2, C_1-C_2 and C_3-C_4 are 3.11, 3.49 and 3.58 kJ/mol respectively. When considering the π bonds C_1-C_6 (2), C_2-C_3 (2) and C_4-C_5 (2) transfer more energy than σ to its π* antibonding orbitals. The transition from πC_1-C_6 is about 21.26 and 17.82 Kcal/mol to the C_2-C_3 and C_4-C_5 acceptor bonds. The other π bonds are πC_2-C_3, C_4-C_5 that transfer 18.61 (C_1-C_6), 22.48 (C_4-C_5) and 22.94 (C_1-C_6), 18.53 kcal/mol (C_2-C_3) respectively. The lone pair atoms sulphur and oxygen are of higher electron density and hence they are not able to have more hyper conjugative interaction energy. The E(2) values and types of the transition are shown in Table.5.

4.5. HOMO LUMO ANALYSIS

The HOMO and the LUMO are very important parameters for quantum chemistry. We can determine the way the molecule interacts with other species; hence, they are called the frontier orbitals. HOMO, which can be thought the outer most orbital containing electrons, tends to transfer these electrons as an electron donor. On the other hand; LUMO can be thought as the inner most orbital containing free places to accept electrons [44]. The HOMO and LUMO energy calculated by B3LYP/6-311/6-311++G(d,p) and HF/6-311++G(d,p) methods are shown in Table.6. This electronic transition absorption corresponds to the transition from the ground to the first excited state and it is mainly described by an electron excitation from the HOMO to the LUMO.

The HOMO is located over the S-CH_3 group and the HOMO → LUMO transition implies an electron density transfer to phenyl ring, which behaves as an acceptor. Energy gap of the frontier orbital has been found and it reveals to be more stable since the shortest band gap is (0.20097 eV). The atomic compositions of the frontier molecular orbitals are shown in Fig.6. The SCF energy of 4-MTA is -61.58 au.

4.6. Molecular Electrostatic Potential

The molecular electrostatic potential isosurface is superimposed on to the total electronic density. The value of the molecular electrostatic potential, V(r), created by a molecular system at a point r gives the electrostatic energy on a unit positive charge located at r. The MEP is a useful property to study reactivity given that an approaching electrophile will be attracted to negative regions (particularly to the points with most negative values), where the electron distribution effect is dominant. Experimental V(r) computed with electron densities obtained from X-ray diffraction data has been used to explore the

(This work is licensed under a Creative Commons Attribution 4.0 International License.)

International Journal of Engineering Research & Technology (IJERT)
ISSN: 2278-0181
Vol. 9 Issue 02, February-2020

electrophilicity of hydrogen bonding functional groups [45]. In the majority of the MEPs, while the maximum positive region which is the preferred site for nucleophilic attack is indicated with blue colour, the maximum negative region which is the preferred site for electrophilic attack is indicated with red colour.

The study of experimental and theoretical V(r) shows that H-donor and H-acceptor properties of molecules are revealed by positive and negative regions, respectively, so that the formation of an H-bond can be regarded as the consequence of a complementarity between the electrostatic potentials [45]. In the present study, the molecular electrostatic potential of 4-MTA is calculated using B3LYP/6-311+G(d,p) method and is depicted in Fig.7. Negative regions are associated with oxygen and sulphur atoms. These are expected to be the most preferred region for electrophilic attack. However, the maximum positive region is localized on carbon and hydrogen. Therefore, it would be predicted that it is the preferred site for nucleophilic attack.

4.7. Other Molecular Properties

4.7.1. Mulliken Charges

The calculation of atomic charges plays an important role in the application of quantum mechanical calculations to molecular systems [46]. The charge distributions calculated by the Mulliken [47] and NBO methods for the equilibrium geometry of 4-MTA is given in Table.7. The charge distribution on the molecule has an important influence on the vibrational spectra. The corresponding Mulliken's plot is shown in Fig.8. In 4-MTA the Mulliken atomic charge of C3 in B3LYP/6-311++G(d,p), shows positive value while it is negative both in HF and NBO. C_{12} possesses more negative charge because the highest electron occupied level is over the S-CH_3 group. Hence it behaves as an electron donor. Since C_1 behaves as an acceptor, it possesses more positive charge.

4.8.1. Thermodynamic Properties

The calculated thermodynamic parameters are presented in the Table.8. Scale factors have been recommended [48] for an accurate prediction in determining the zero-point vibrational energies and the entropy S. The variation in the zero-point vibrational energies seems to be insignificant. The total energies were found to decrease with increase of the basis sets. The changes in the total entropy of 4-MTA at room temperature at different basis sets are only marginal.

5. CONCLUSION

In this work, 4-MTA has been characterized by NMR, FT-IR, FT-Raman, HOMO, LUMO and NBO analysis. The energies, geometrical parameters, vibrational frequencies and ^{13}C /^{1}H chemical shift values of the title compound were calculated using *ab initio* and DFT/B3LYP at the several basis set levels. Correlations between the proton and ^{13}C experimental chemical shifts and the GIAO NMR calculations are found to be in good agreement. The molecular electrostatic potential of 4-MTA reveals the most preferred region for electrophilic attack and it is found to be over the negative regions associated with oxygen and sulphur atoms. In addition, the thermodynamic, Mulliken charges, non-linear optical, total dipole moment and first order hyperpolarizabilities properties of the compound have been calculated in order to get an insight into the compound.

Acknowledgments

The computations were partially done by K. Drużbicki at the Academic Computer Centre CYFRONET AGH, Cracow, Poland (Grant number: MNiSW/SGI3700/UJ/007/2009). Our hearty thanks also goes to Yusuf Erdogdu, Department of Physics, Faculty of Arts and Science, Ahi Evran University, Kirsehir, Turkey and Tom Sundius, Department of Physics, University of Helsinki, FIN-00014, Finland for timely help and constant support in completion of this work.

REFERENCES:

[1] G.M. Anderson, P.A. Kollman, L.N. Domelsmith, K.N. Houk, J. Am. Chem. Soc. 101 (1979) 2344.
[2] P.J. Breen, E.R. Bernstein, H.V. Secor, J.I. Seeman, J. Am. Chem. Soc. 111 (1989) 1958.
[3] C.G. Eisenhardt, G. Pietraperzia, M. Becucci, Phys. Chem. Chem. Phys. 3 (2001) 1407.
[4] W.J. Balfour, Spectrochim. Acta 39A (1983) 795.
[5] V. Ashok Babu, B. Lakshmaiah, K. Sree Ramulu, G. Ramana Rao, Ind. J. Pure Appl. Phys. 25 (1987) 58.
[6] J.A. Tossell, M.D. Zimmermann, Cosmochim. Acta 72 (2008) 5232.
[7] Mariko Nagasaka-Hoshino, Tasuku Isozaki, Tadashi Suzuki, Teijiro Ichimura, Susumu Kawauchi, Chem. Phys. Lett. 457 (2008) 58.
[8] Jiangou Huang, Wenbih Tzeng, Spectrochim. Acta 67A (2007) 824.
[9] V. Krishnakumar, R. Ramasamy, Spectrochim. Acta 62A (2005) 570.
[10] Mario Bossa, Simone Morpurgo, Stefano Stranges, J. Mol. Str. (THEOCHEM) 618 (2002) 155.
[11] B. Venkatram Reddy and G. Ramana Rao, Vib. Spectrosc. 6 (1994) 251.
[12] B. Lakshmaiah, G. Ramana Rao, J. Raman Spectrosc. 20 (1989) 439.
[13] H. Tylli, H. Konschin, C. Grundfelt-Forsius, J. Mol. Struct. 55 (1979) 157.
[14] Gaussian 09, Revision A.02, Wallingford CT, 2009.
[15] H.B. Schlegel, J. Comput. Chem. 3 (1982) 214.
[16] T. Sundius, J. Mol. Struct. 218 (1990) 321
[17] T. Sundius, Vib. Spectrosc. 29 (2002) 89–95. (b) MOLVIB (v.7.0): Calculation of Harmonic Force Fields and Vibrational Modes of Molecules, QCPE program No. 807 (2002).
[18] G. Fogarasi, P. Pulay, in: J.R. Durig (Ed.), Vibrational Spectra and Structure, vol. 14, Elsevier,Amsterdam, 1985, pp. 125–219,Chapter 3.
[19] P. Pulay, G. Fogarasi, X. Zhou, P.W. Taylor, Vib. Spectrosc.1 (1990) 159.
[20] G. Fogarasi, X. Zhou, P.W. Taylor, P. Pulay, J. Am. Chem. Soc. 114 (1992) 8191.
[21] G.Kerestury, S.Holly, J. Varga, G. Besenyi, A. Wang, J.R. Durig, Spectrochim. Acta 49A (1993) 2007.
[22] J. Baker, A.A. Jarzecki, P. Pulay, J. Phys. Chem. A 102 (1998) 1412.

(This work is licensed under a Creative Commons Attribution 4.0 International License.)

International Journal of Engineering Research & Technology (IJERT)
ISSN: 2278-0181
Vol. 9 Issue 02, February-2020

[23] V. Krishnakumar, G. Keresztury, T. Sundius, R. Ramasamy, J. Mol. Struct. 702 (2004) 9.
[24] R. Korlacki, K. Merkel, J.K. Vij, R. Wrzalik, A. Kocot, M.D.Ossowska- Chruściel, J. Chruściel, S. Zalewski, Liquid Crystals 33 (2006) 219.
[25] M. P. Andersson, P. Uvdal, J. Phys. Chem. A 109 (2005) 2937.
[26] D.A.Kleinman, Phys. Rev 126 (1962) 1977.
[27] Igor F. Shishkov, Lyudmila V. Khristenko, Nikolai M. Karasev, Lev V. Vilkov, Heinz Oberhammer, J. Mol. Struct. 873 (2008) 137.
[28] G. Varsanyi, Assignments for vibrational spectra of seven hundred Benzene Derivatives, Vol.1- 2, Academiai Kiado, Budapest, 1973.
[29] A. J. Barnes, M. A. Majid, M. A. Stuckey, P. Gregory, C. V. Stead, Spectrochim. Acta 41(1985) 629.
[30] C. Sourisseau, P. Maraval, J. Raman Spectrosc. 25 (1994) 477.
[31] G. Socrates, Infrared Characteristic Group frequencies, Wiley, Interscience Publication, New York (1980).
[32] L.J. Bellamy, The Infrared Spectra of Complex Molecules, John Wiley, New York, 1959.
[33] J. Swaminathan, M. Ramalingam, H. Saleem, V. Sethuraman, M.T. Noorul Ameeen, Spectrochim. Acta 74A (2009) 1247.
[34] S.J. Bunce, H.G.M. Edwards, A.F. Johnson, I.R. Lewis, P.H. Turner, Spectrochim. Acta 49A (1993) 775.
[35] B. Venkatram Reddy and G. Ramana Rao,Vib. Spectrosc. 6 (1994) 231.
[36] J.F. Arenas, I. López Tocón, J.C. Otero, J.I. Marcos, J. Mol. Struct. 476 (1999) 139.
[37] D.A. Long, W.O. George, Spectrochim. Acta 19 (1963) 1777.
[38] S. Sebastian, N. Sundaraganesan, S. Manoharan, Spectrochim. Acta 74A (2009) 312.
[39] K.C. Medhi, R. Barman, M.K. Sharma, Indian. J. Phys. 68B (1994) 189.
[40] M. Szafran, A. Komasa, E. Bartoszak-Adamska, J. Mol. Struct. 827 (2007) 101.
[41] C. James, A. Amal Raj, R. Reghunathan, V.S. Jayakumar, I. Hubert Joe, J. Raman Spectrosc. 37 (2006) 1381.
[42] Liu Jun-na, Chen Zhi-rong, Yuan Shen-fang, J. Zhejiang. Univ. Sci. 6B (2005) 584.
[43] S. Sebastian, N. Sundaraganesan, Spectrochim. Acta 75A (2010) 941.
[44] G. Gece, Corros. Sci. 50 (2008) 2981.
[45] S.J. Grabowski, J. Leszczynski, Unrevealing the nature of hydrogen bonds: p-electron delocalization shapes H-bond features, in: J. Slawomir (Ed.), Hydrogen Bonding -New Insights, Grabowski Kluwer, Academic Publishers, 2006.
[46] S. Gunasekaran, S. Kumaresan, R. Arunbalaji, G. Anand, S. Srinivasan, J. Chem. Sci. 120 (2008) 315.
[47] R.S. Mulliken, J. Chem. Phys. 23 (1955) 1833.
[48] Mauricio Alcolea Palafox, Int. J. Quantum. Chem. 77 (2000) 661.

List of Figures

Fig.1

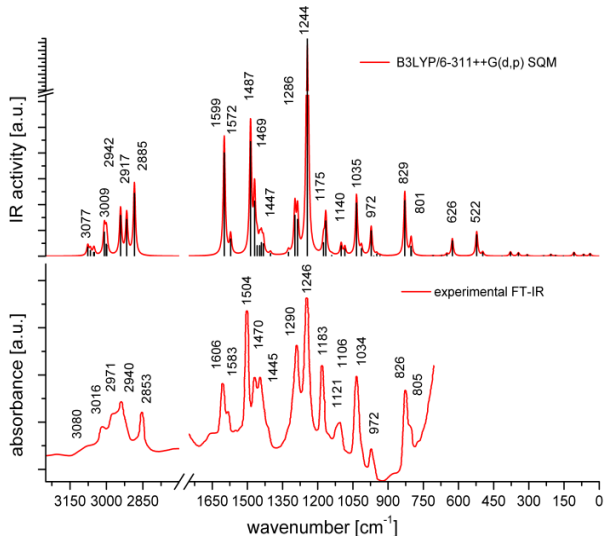

Fig.2

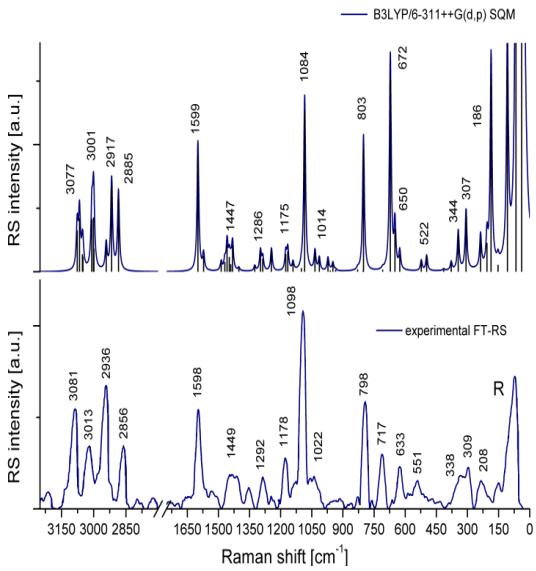

Fig.3

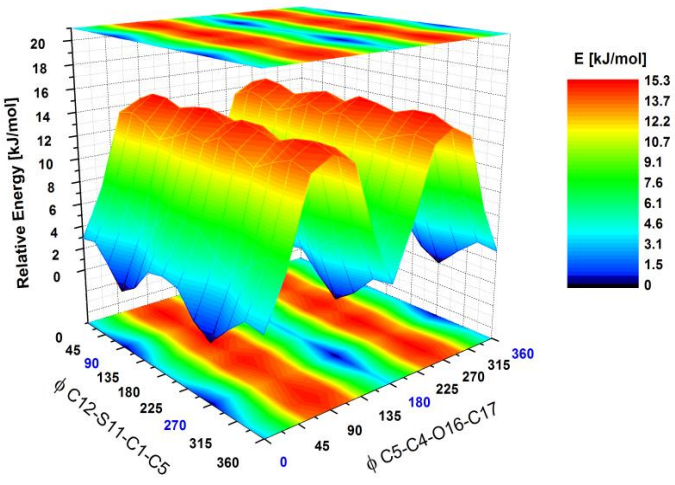

Fig.4

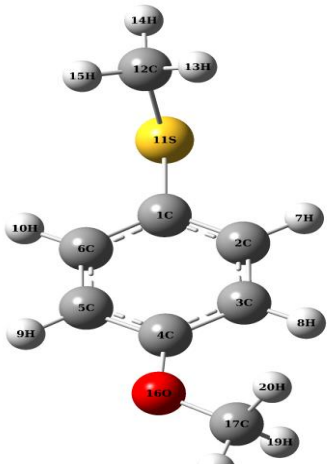

(This work is licensed under a Creative Commons Attribution 4.0 International License.)

International Journal of Engineering Research & Technology (IJERT)
ISSN: 2278-0181
Vol. 9 Issue 02, February-2020

Fig.5 (a)

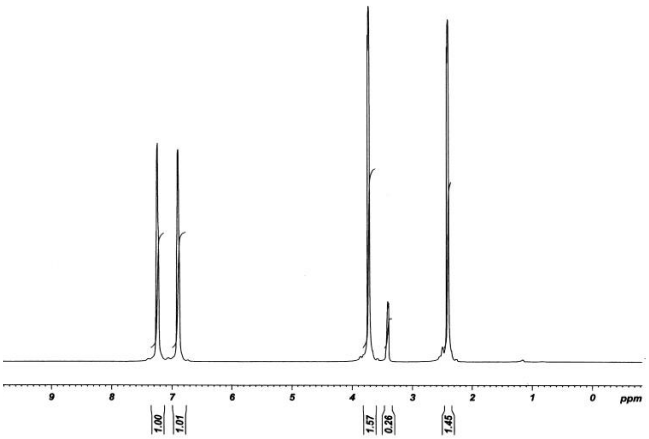

(b)

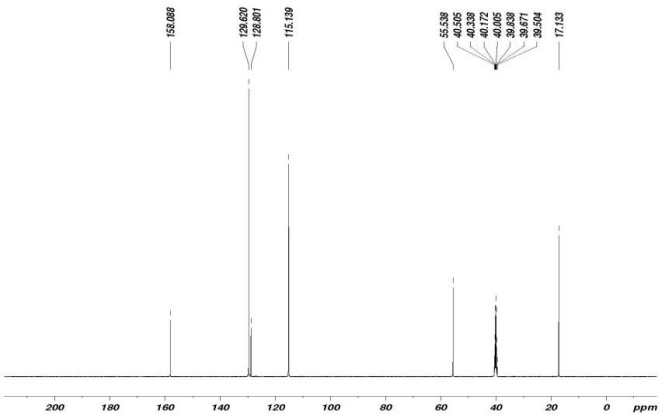

Fig.6 HOMO

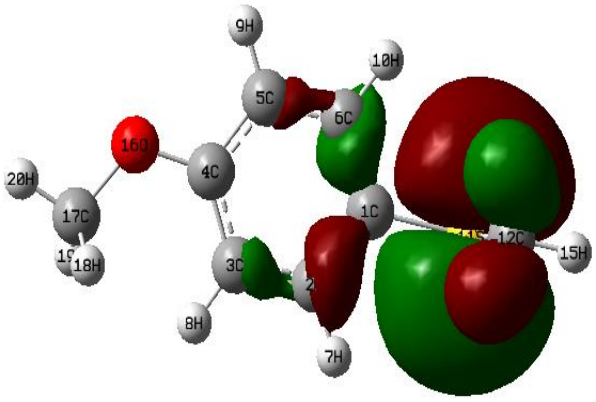

LUMO

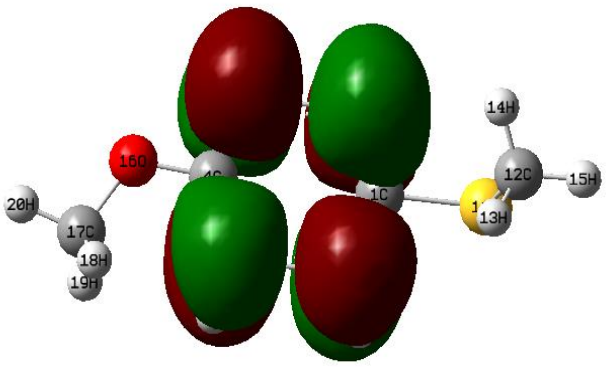

Fig.7

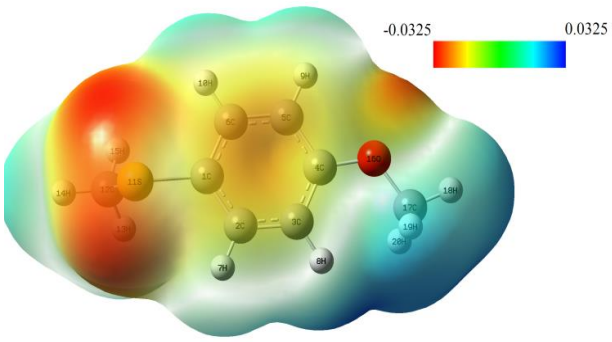

Fig.8

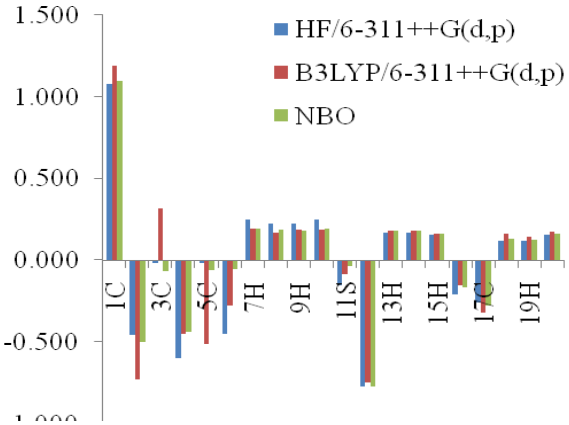

(This work is licensed under a Creative Commons Attribution 4.0 International License.)

International Journal of Engineering Research & Technology (IJERT)
ISSN: 2278-0181
Vol. 9 Issue 02, February-2020

List of Tables:

Table.1.Definition of internal valence coordinates of 4-MTA.

No. (i)	Symbol	Type	Definition
		Stretching	
1-4	r_i	C–H (aromatic)	H7-C2, H8-C3, H9-C5, H10-C6
5–7	r_i	C–H (methyl a)	H13-C12, H14-C12, H15-C12
8-10	r_i	C–H (methyl b)	H18-C17, H19-C17, H20-C17
11-12	Q_i	C–S, S–C (metyl a)	C12-S11, S11-C1
13-14	Q_i	C–O, O–C (metyl b)	C17-O16, O16-C4
15-20	R_i	C–C (aromatic)	C1-C2, C2-C3, C3-C4, C4-C5, C5-C6, C6-C1
		Bending	
21-28	β_i	C–C–H	C1-C2-H7, C3-C2-H7, C2-C3-H8, C4-C3-H8, C4-C5-H9, C6-C5-H9, C5-C6-H10, C1-C6-H10
29-31	β_i	S-C-H	S11-C12-H13, S11-C12-H14, S11-C12-H15,
32-34	α_i	H-C-H (metyl a)	H13-C12-H15, H14-C12-H15, H14-C12-H13
35-37	β_i	O-C-H	O16-C17-H18, O16-C17-H19, O16-C17-H20
38-40	α_i	H-C-H (metyl b)	H18-C17-H20, H19-C17-H20, H19-C17-H18
41-42	δ_i	C–C–S	C2-C1-S11, C6-C1-S11
43-44	δ_i	C–C–O	C3-C4-O16, C5-C4-O16
45	σ_i	C–S–C	C12-S11-C1
46	σ_i	C–O–C	C17-O16-C4
47-52	γ_i	C–C–C	C2-C1-C6, C1-C6-C5, C6-C5-C4, C5-C4-C3, C4-C3-C2, C3-C2-C1
		Out-of-plane bending (wagging)	
53-56	ω_i	C_{ar} –H	H10-C6-C1-C5,H9-C5-C6-C4, H8-C3-C4-C2,H7-C2-C3-C1
57	ω_i	C_{ar} –S	S11-C1-C6-C2
58	ω_i	C_{ar} –O	O16-C4-C5-C3
		Torsion	
59	τ_i	τC_{ar} –S	C12-S11-C1-(C2,C6)
60	τ_i	τC_{ar} –O	C17-O16-C4-(C3,C5)
61	τ_i	τS–CH_3	(H13, H14, H15)-C12-S11-C1
62	τ_i	τO–CH_3	(H18, H19, H20)-C17-O16-C4
63-68	τ_i	τC–C (ring)	C3-C4-C5-C6, C4-C5-C6-C1, C5-C6-C1-C2, C6-C1-C2-C3, C1-C2-C3-C4, C2-C3-C4-C5

(This work is licensed under a Creative Commons Attribution 4.0 International License.)

International Journal of Engineering Research & Technology (IJERT)
ISSN: 2278-0181
Vol. 9 Issue 02, February-2020

Table.2.Definition of local symmetry coordinates and the values of corresponding scale factors (S_i) used to correct the B3LYP/double- and triple-ζ force fields.

No. (i)	Symbol[a]	Definition[b]	The scale factors (S_i) applied in the calcul		
			6-31G(d)	6-31+G(d)	6-311+G(d,p)
1–4	νCH$_{ar}$	r_1, r_2, r_3, r_4	0.920	0.915	0.9265
5	νCH$_3$ss (a)	$(r_5 + r_6 + r_7)/\sqrt{3}$	0.920	0.889	0.919
6	νCH$_3$ips (a)	$(2r_5 - r_6 - r_7)/\sqrt{6}$	0.920	0.889	0.919
7	νCH$_3$ops (a)	$(r_5 - r_6)/\sqrt{2}$	0.920	0.889	0.919
8	νCH$_3$ss (b)	$(r_8 + r_9 + r_{10})/\sqrt{3}$	0.920	0.889	0.919
9	νCH$_3$ips (b)	$(2r_8 - r_9 - r_{10})/\sqrt{6}$	0.920	0.889	0.919
10	νCH$_3$ops (b)	$(r_8 - r_9)/\sqrt{2}$	0.920	0.889	0.919
11-12	νC$_{ar}$S, SC	Q_{11}, Q_{12}	0.922	0.9254	1.024
13-14	νC$_{ar}$O, OC	Q_{13}, Q_{14}	0.922	0.9254	1.024
15-20	νCC$_{ar}$	$R_{15}, R_{16}, R_{17}, R_{18}, R_{19}, R_{20}$	0.922	0.9254	0.954
21-24	δCH$_{ar}$	$(\beta_{21} - \beta_{22})/\sqrt{2}, (\beta_{23} - \beta_{24})/\sqrt{2}, (\beta_{25} - \beta_{26})/\sqrt{2}, (\beta_{27} - \beta_{28})/\sqrt{2},$	0.950	0.9473	0.977
25	δCH$_3$sb (a)	$(-\beta_{29} - \beta_{30} - \beta_{31} + \alpha_{32} + \alpha_{33} + \alpha_{34})/\sqrt{6}$	0.915	0.9171	0.9405
26	δCH$_3$ipb (a)	$(-\alpha_{32} - \alpha_{33} + 2\alpha_{34})/\sqrt{6}$	0.915	0.9171	0.9405
27	δCH$_3$opb (a)	$(-\alpha_{32} - \alpha_{33})/\sqrt{2}$	0.915	0.9171	0.9405
28	ρSCH$_3$ipr	$(2\beta_{29} - \beta_{30} - \beta_{31})/\sqrt{6}$	0.950	0.9473	0.938
29	ρSCH$_3$opr	$(\beta_{30} - \beta_{31})/\sqrt{2}$	0.950	0.9473	0.938
30	δCH$_3$sb (b)	$(-\beta_{35} - \beta_{36} - \beta_{37} + \alpha_{38} + \alpha_{39} + \alpha_{40})/\sqrt{6}$	0.915	0.9171	0.9405
31	δCH$_3$ipb (b)	$(-\alpha_{38} - \alpha_{39} + 2\alpha_{40})/\sqrt{6}$	0.915	0.9171	0.9405
32	δCH$_3$opb (b)	$(-\alpha_{38} - \alpha_{39})/\sqrt{2}$	0.915	0.9171	0.9405

Table.2 (continued)...

No. (i)	Symbol[a]	Definition[b]	The scale factors applied in the calculations*		
33	ρOCH$_3$ipr	$(2\beta_{35} - \beta_{36} - \beta_{37})/\sqrt{6}$	0.950	0.9473	0.938
34	ρOCH$_3$opr	$(\beta_{36} - \beta_{37})/\sqrt{2}$	0.950	0.9473	0.938
35	δCS	$(\delta_{41} - \delta_{42})/\sqrt{2}$	0.990	0.9923	1.009
36	δCO	$(\delta_{43} - \delta_{44})/\sqrt{2}$	0.990	0.9923	1.009
37	δCSC	σ_{45}	0.990	0.9923	1.009
38	δCOC	σ_{46}	0.990	0.9923	1.009
39	Rtrigd	$(\gamma_{47} - \gamma_{48} + \gamma_{49} - \gamma_{50} + \gamma_{51} - \gamma_{52})/\sqrt{6}$	0.990	0.9923	0.966
40	Rsymd	$(-\gamma_{47} - \gamma_{48} + 2\gamma_{49} - \gamma_{50} - \gamma_{51} + 2\gamma_{52})/\sqrt{12}$	0.990	0.9923	0.966
41	Rasyd	$(\gamma_{47} - \gamma_{48} + \gamma_{50} - \gamma_{51})/2$	0.990	0.9923	0.966
42-45	γCH$_{ar}$	$\omega_{53}, \omega_{54}, \omega_{55}, \omega_{56}$	0.976	0.9711	0.962
46	γCS	ω_{57}	0.976	0.9711	1.007
47	γCO	ω_{58}	0.976	0.9711	1.007
48	τCS	τ_{59}	0.831	0.8980	0.831
49	τCO	τ_{60}	0.831	0.8980	0.831

(This work is licensed under a Creative Commons Attribution 4.0 International License.)

International Journal of Engineering Research & Technology (IJERT)
ISSN: 2278-0181
Vol. 9 Issue 02, February-2020

50	τCH3 (a)	τ_{61}	0.831	0.8980	0.831
51	τCH3 (b)	τ_{62}	0.831	0.8980	0.831
52	τRtrig	$(\tau_{63} - \tau_{64} + \tau_{65} - \tau_{66} + \tau_{67} - \tau_{68})/\sqrt{6}$	0.935	0.8980	0.896
53	τRsym	$(\tau_{63} - \tau_{65} + \tau_{66} - \tau_{68})/2$	0.935	0.8980	0.896
54	τRasy	$(-\tau_{63} + 2\tau_{64} - \tau_{65} - \tau_{66} + 2\tau_{67} - \tau_{68})/\sqrt{12}$	0.935	0.8980	0.896

(S_i) 6-31G(d), 6-311+G(d,p) according to Pulay and Fogarasi [19,20] and Krishnakumar [23]; 6-31+G(d) according to Korlacki [24]. 6-311++G(d,p) in this work was refined from the quoted 6-31G(d) scale factors.

Table.3. Calculated electric dipole moments μ (Debye), dipole moment conponents, β components and β_{tot} value of 4-MTA.

Parameters	B3LYP/6-31G(d,p)
μ_x	0.4505
μ_y	-0.5404
μ_z	0.7661
μ	1.0402
βxxx	-208.8353
βxxy	-28.5950
βxyy	-27.0431
βyyy	-15.4580
βxxz	-190.0055
βxyz	-17.1981
βyyz	21.9882
βxzz	-90.1606
βyzz	-20.7562
βzzz	23.9372
$\beta_{total\ (esu)}$	3.1300×10^{-30}

Table.4.Theoretical and experimental ^{1}H and ^{13}C spectra of 4-MTA (with respect to TMS, all values in ppm).

Atoms	B3LYP/6-311++G(d,p)	Experimental
C_4	167.44	158.09
C_2	142.84	115.14
C_6	142.33	115.14
C_1	136.86	128.80
C_5	122.43	129.62
C_3	113.13	129.62
C_{17}	55.40	55.54
C_{12}	28.11	17.13
H_7	7.77	7.23
H_{10}	7.75	7.23
H_9	7.13	6.89
H_8	6.92	6.89
H_{20}	4.08	3.72
H_{19}	3.74	3.72
H_{18}	3.72	3.72
H_{14}	2.36	2.41
H_{13}	2.26	2.41
H_{15}	2.02	2.41

(This work is licensed under a Creative Commons Attribution 4.0 International License.)

International Journal of Engineering Research & Technology (IJERT)
ISSN: 2278-0181
Vol. 9 Issue 02, February-2020

Table.5. Second order perturbation theory anlaysis of Fock matrix in NBO basis for 4-MTA using B3LYP/6-311++G(d,p).
using B3LYP/6-311++G(d,p).

Donor (i)	Type	ED/e	Acceptor (j)	Type	ED/e	E(2)[a] (kJmol^{-1})	E(j)-E(i)[b] (a.u)	F(i,j)[c] (a.u)
C1-C6 (1)	σ	1.979	C1-C2	σ*	0.030	3.11	1.28	0.06
			C2-H7		0.015	2.46	1.16	0.05
			C5-C6		0.017	3.01	1.29	0.06
C1-C6 (2)	π	1.675	C2-C3 (2)	π*	0.320	21.26	0.29	0.07
			C4-C5 (2)		0.361	17.82	0.29	0.06
C1-S11	σ	1.977	C2-C3	σ*	0.017	3.16	1.19	0.06
			C5-C6		0.017	3.18	1.19	0.06
C2-C3 (1)	σ	1.972	C1-C2	σ*	0.030	3.49	1.27	0.06
			C1-S11		0.030	4.24	0.90	0.06
C2-C3 (2)	π	1.669	C1-C6 (2)	π*	0.375	18.61	0.28	0.07
			C4-C5 (2)		0.361	22.48	0.28	0.07
C3-H8		1.977	C1-C2		0.030	3.58	1.09	0.06
			C4-C5		0.030	4.25	1.09	0.06
C4-C5 (1)	σ	1.977	C3-C4	σ*	0.030	3.58	1.28	0.06
C4-C5 (2)	π	1.648	C1-C6 (2)	π*	0.375	22.94	0.28	0.07
			C2-C3 (2)		0.320	18.53	0.29	0.07
C5-H9		0.013	C1-C6		0.030	3.57	1.09	0.06
			C3-C4		0.030	4.24	1.09	0.06
C6-H10		0.015	C1-C2		0.030	4.46	1.09	0.06
			C4-C5		0.030	3.47	1.09	0.06
O16-C17 (1)	σ		C4-C5	σ*	0.030	0.66	1.36	0.03
			C4-C5 (2)		0.361	2.61	0.82	0.05
LPS 11 (1)	σ	1.975	C1-C2		0.030	1.61	1.19	0.04
LPS 11 (2)	π	1.935	C1-C2	π*	0.030	4.83	0.80	0.06
			C1-C6		0.030	4.83	0.80	0.05
LP O 16 (1)	σ	1.939	C12-H13	σ*	0.016	4.20	0.63	0.05
			C12-H14		0.016	4.20	0.63	0.05
			C3-C4		0.030	3.20	0.93	0.05
			C4-C5		0.030	7.18	0.93	0.05
			C4-C5 (2)		0.361	2.73	0.39	0.03
LP O 16 (2)	π	1.934	C3-C4	π*	0.030	3.88	1.06	0.06
			C4-C5 (2)		0.361	5.12	0.52	0.05
			C17-H18		0.020	3.97	0.87	0.05

[a] E(2) means energy of hyper conjugative interaction (stabilization energy)
[b] Energy difference between donor and acceptor i and j NBO orbitals.
[c] F(i,j) is the Fock matrix element between i and j NBO orbitals.

Table.6. HOMO LUMO energy calculated by HF and DFT methods.

Parameter	HF/6-311++G(d,p) (a.u)	B3LYP/6-311G(d,p) (a.u)	B3LYP/6-311++G(d,p) (a.u)
Homo	-0.33069	-0.23145	-0.23252
LUMO	0.03808	-0.02574	-0.03155
Energy gap (ΔE)	0.29261	0.20571	0.20097

(This work is licensed under a Creative Commons Attribution 4.0 International License.)

International Journal of Engineering Research & Technology (IJERT)
ISSN: 2278-0181
Vol. 9 Issue 02, February-2020

SCF energy = -784.39 a.u.

Table.7. Calculated Mulliken charges of 4-MTA.

Charges	HF/6-311++G(d,p)	B3LYP/6-311++G(d,p)	NBO
1C	1.078	1.193	1.099
2C	-0.454	-0.725	-0.496
3C	-0.018	0.320	-0.066
4C	-0.596	-0.451	-0.434
5C	-0.014	-0.514	-0.061
6C	-0.451	-0.275	-0.0510
7H	0.248	0.195	0.194
8H	0.227	0.167	0.189
9H	0.228	0.189	0.184
10H	0.248	0.191	0.194
11S	-0.154	-0.084	-0.033
12C	-0.770	-0.747	-0.768
13H	0.169	0.1833	0.180
14H	0.169	0.179	0.180
15H	0.157	0.162	0.166
16O	-0.209	-0.154	-0.163
17C	-0.256	-0.317	-0.273
18H	0.118	0.163	0.130
19H	0.119	0.147	0.125
20H	0.157	0.178	0.164

Table.8. Theoretically computed energies, zero-point vibrational energies, rotational constants, entropies and dipole moment for 4-MTA.

Parameters	HF/6-311++G(d,p)	B3LYP/6-311G(d,p)	B3LYP/6-311++G(d,p)
Total Energies (a.u)	-781.23	-784.39	-784.39
Zero point energy (kcal/mol)	107.49	101.01	100.90
Rotational constants (GHz)	3.72	3.54	3.54
	0.54	0.53	0.53
	0.51	0.50	0.50
Entropy (cal/mol/K)			
Total	102.77	101.30	101.21
Translational	41.01	41.01	41.01
Rotational	30.13	30.21	30.21
Vibrational	31.63	30.08	29.99
Dipole moment (D)	0.98	1.16	0.95

(This work is licensed under a Creative Commons Attribution 4.0 International License.)